
A numerical light curve model for interaction-powered supernovae

Yuki TAKEI,^{1,2,3,*} and Toshikazu SHIGEYAMA^{1,2}

¹Research Center for the Early Universe (RESCEU), Graduate School of Science, The University of Tokyo, 7-3-1 Hongo, Bunkyo-ku, Tokyo 113-0033, Japan

²Department of Astronomy, Graduate School of Science, The University of Tokyo, 7-3-1 Hongo, Bunkyo-ku, Tokyo 113-0033, Japan

³Astrophysical Big Bang Laboratory, RIKEN, 2-1 Hirosawa, Wako, Saitama 351-0198, Japan

*E-mail: takei@resceu.s.u-tokyo.ac.jp

Received ; Accepted

Abstract

We construct a numerical light curve model for interaction-powered supernovae that arise from an interaction between the ejecta and the circumstellar matter (CSM). In order to resolve the shocked region of an interaction-powered supernova, we solve the fluid equations and radiative transfer equation assuming the steady states in the rest frames of the reverse and forward shocks at each time step. Then we numerically solve the radiative transfer equation and the energy equation in the CSM with the thus obtained radiative flux from the forward shock as a radiation source. We also compare results of our models with observational data of two supernovae 2005kj and 2005ip classified as type IIn and discuss the validity of our assumptions. We conclude that our model can predict physical parameters associated with supernova ejecta and the CSM from the observed features of the light curve as long as the CSM is sufficiently dense. Furthermore, we found that the absorption of radiation in the CSM is an important factor to calculate the luminosity.

Key words: supernovae: general — supernovae: individual (SN 2005kj, SN 2005ip) — circumstellar matter — stars: mass-loss — shock waves

1 Introduction

Supernovae (SNe) show various properties in their spectra and light curves (LCs) strongly depending on how their progenitors have evolved. Massive stars are known to lose their own envelopes due to the radiation pressure throughout their lives (e.g., Castor, Abbott, & Klein 1975; Smith & Owocki 2006), leading to the formation of circumstellar matter (CSM) with a variety of density structures (see Smith 2014). Especially, some progenitors seem to experience extremely intense mass-loss events shortly before the explosion, which results in the formation of dense CSM. If a massive star explodes as a SN in the CSM rich in hydrogen, some photons emitted from the SN are scattered by or ionize hydrogen atoms in the dense CSM and form narrow hydrogen emission lines in the spectrum. Such a SN was classified as type IIn by Schlegel (1990) (see also Filippenko 1997). One of the highly important features of SNe IIn is an interaction between ejecta and CSM which dissipates the kinetic energy in the ejecta to the radiation energy. In addition, the dense CSM may delay the emergence of a shock wave propagating in the envelope of the progenitor (e.g., Chevalier & Irwin 2011) and in fact the delay of the shock breakout occurs in most SNe II (Förster et al. 2018). Therefore, we can extract some useful pieces of information about CSM from LCs of SNe IIn in the early brightening phases. Studying LCs of SNe IIn is of significance in understanding the mass-loss history of progenitors, which may tell us about the final stage of the evolution of massive stars. This will also help to test theoretical models for the evolution of massive stars shortly before the core-collapse.

Many investigations into LCs of SNe IIn have been done analytically, semi-analytically, and numerically (e.g., Ginzburg & Balberg 2012; Chatzopoulos et al. 2012; Moriya et al. 2013b; Dessart et al. 2015; Tsuna et al. 2019). Moriya et al. (2013b) analytically derived the radius of the shocked region as a function of time and obtained bolometric LC of SN IIn assuming that a cool dense shell is formed between SN ejecta and CSM due to the efficient radiative cooling. Ginzburg & Balberg (2012); Tsuna et al. (2019) used the self-similar solution by Chevalier (1982) for a shocked region, and conduct radiative transfer calculations in the shocked region and the unshocked CSM. Chatzopoulos et al. (2012) applied the model of Arnett (1980) that presents analytical formulae expressing LCs of SNe II-P and II-L to SN IIn, and calculated the luminosity of SN IIn numerically. Dessart et al. (2015) carried out multi-group radiation hydrodynamical calculations for SNe interacting with the CSM to investigate the origin of some types of super-luminous SNe.

As these models do not resolve the shocked region efficiently or do not solve the

structure by consistently taking into account the effects of radiation, here we present an alternative way to guarantee the spatial resolution in the shocked region. This method is not restricted to the power law density structures, which are necessary assumptions in some of the previous works mentioned above. We show that we can determine the distributions of physical quantities between the two shocks as functions of time assuming a steady state in the rest frame of each of the shocks at each time step for given ejecta and the CSM structures. Then we can calculate the LC by solving the radiative transfer equation and energy equation in the CSM ahead of the forward shock with the radiative flux from the forward shock as the inner boundary condition.

This paper is organized as follows; In section 2, we formulate our model including the inner and outer boundary conditions. Then we present results of our model, compare them with the observational data of SNe 2005kj and 2005ip, and discuss the validity of some of our assumptions in section 3. Finally, we conclude the paper in section 4.

2 Model

After an explosion, a collision between SN ejecta and dense CSM results in the formation of a forward shock propagating in the CSM and a reverse shock propagating in the SN ejecta. This shocked region is composed of two components, shocked SN ejecta and shocked CSM, separated by a contact discontinuity. In this section, we explain how we calculate spherically symmetric structures in these two shocked regions and derive the emergent radiative flux as a function of time and radius. Then we describe radiative transfer calculations in the unshocked CSM heated by the radiative flux emergent from the shocked region. In the following, a subscript r_s (f_s) denotes physical quantities at the reverse (forward) shock.

2.1 Shocked region

Assuming a steady state in the rest frame of each of the shocks, we calculate the distributions of physical quantities in this region by integrating the following equations with respect to the radius r .

$$\frac{\partial(r^2\rho v)}{r^2\partial r} = 0, \quad (1)$$

$$v\frac{\partial v}{\partial r} + \frac{1}{\rho}\frac{\partial p}{\partial r} = 0, \quad (2)$$

$$\frac{\partial}{r^2\partial r} \left[r^2 \left\{ \rho v \left(\frac{1}{2}v^2 + e + \frac{p}{\rho} \right) + F \right\} \right] = 0, \quad (3)$$

where v denotes the velocity in the rest frame of each of the shocks, ρ the density, p the pressure, e the specific internal energy, and F denotes the radiative flux. The velocity v in the rest frame of the shock is transformed to $v + u$ in the rest frame of the center of the coordinate system ($r = 0$), where u is the shock velocity in the same frame. Here we have assumed that the shocked region is in local thermodynamic equilibrium (LTE) state to avoid numerical instabilities associated with the integration. Thus we use the following equation of state,

$$p = \frac{\rho}{\mu m_{\text{u}}} kT + \frac{1}{3} a T^4, \quad (4)$$

where μ is the mean molecular weight, T the temperature, m_{u} the atomic mass unit, k the Boltzmann constant, and a the radiation constant. μ becomes about 0.62 in fully ionized gases composed of the solar abundances of elements. We fix $\mu = 0.62$ in the shocked region. Then the specific internal energy e is given as

$$\rho e = \frac{3}{2} \frac{\rho}{\mu m_{\text{u}}} kT + a T^4. \quad (5)$$

Though this assumption of LTE is eventually broken at later epochs when the shocked region becomes optically thin and the radiation temperature could deviate from the gas temperature, we can assume LTE at earlier epochs when the shocked region is optically thick. We will check the validity of this assumption for actual results presented in the next section.

When the shocked region is optically thick, we can apply the diffusion approximation to calculate F ,

$$F = - \frac{ac}{3(\kappa + \sigma)\rho} \frac{\partial T^4}{\partial r}, \quad (6)$$

where κ and σ are the absorption coefficient and the scattering coefficient, and c is the speed of light. We use the Rosseland mean opacity presented by Iglesias & Rogers (1996) that covers the temperature range of $3.75 \leq \log T(\text{K}) \leq 8.70$ (OPAL opacity code). In the lower temperature range of $3.20 \leq \log T(\text{K}) \leq 3.75$, we use the opacity presented by Marigo & Aringer (2009).

2.2 Initial conditions and boundary conditions

Assuming that homologously expanding SN ejecta have a density profile $\rho_{\text{ej}}(r, t)$ with a broken power-law, one obtains

$$\rho_{\text{ej}}(r, t)$$

$$= \begin{cases} \frac{1}{4\pi(n-\delta)} \frac{[2(5-\delta)(n-5)E_{\text{ej}}]^{(n-3)/2}}{[(3-\delta)(n-3)M_{\text{ej}}]^{(n-5)/2}} t^{-3} \left(\frac{r}{t}\right)^{-n} & (r \geq v_t), \\ \frac{1}{4\pi(n-\delta)} \frac{[2(5-\delta)(n-5)E_{\text{ej}}]^{(\delta-3)/2}}{[(3-\delta)(n-3)M_{\text{ej}}]^{(\delta-5)/2}} t^{-3} \left(\frac{r}{t}\right)^{-\delta} & (r \leq v_t), \end{cases} \quad (7)$$

for a given ejecta mass M_{ej} and kinetic energy E_{ej} of the ejecta (Matzner & McKee 1999). Here v_t is determined so that the density be continuous at $r/t = v_t$. The exponent n depends on the envelope structure of the progenitor. The explosion of a blue super-giant (BSG) (a red super-giant (RSG)) gives $n \simeq 10$ ($\simeq 12$). The slope δ in the inner region takes a value in the range $0 - 1$. We assume that the CSM density profile follows $\rho_{\text{CSM}} \propto r^{-s}$. We constrain $s < 3$, because $s \geq 3$ gives a solution in which the shock front is accelerating (Chevalier 1982). When we use the density profile with $s = 2$, which describes a steady mass-loss with a constant mass-loss rate and wind velocity, we set the wind velocity v_w to be 100 km s^{-1} for simplicity. The Rankine-Hugoniot conditions relate physical quantities in the upstream (with subscript 0) of a shock wave to those in the downstream (with subscript 1) by the following equations,

$$\rho_0 v_0 = \rho_1 v_1, \quad (8)$$

$$\rho_0 v_0^2 + p_0 = \rho_1 v_1^2 + p_1, \quad (9)$$

$$\frac{1}{2} v_0^2 + e_0 + \frac{p_0}{\rho_0} + \frac{F_0}{\rho_0 v_0} = \frac{1}{2} v_1^2 + e_1 + \frac{p_1}{\rho_1} + \frac{F_1}{\rho_1 v_1}. \quad (10)$$

As the mean free path of photons is much longer than that of gas particles, it is reasonable to assume that F_0 and F_1 take the same value.

In order to start the calculation of the inner structure of the shocked region from an initial time $t = t_{\text{ini}}$, we first fix the initial radius of the reverse shock $r_{\text{rs}}(t_{\text{ini}})$ that can be obtained by the thin shell approximation (Moriya et al. 2013b). The radius of the forward shock $r_{\text{fs}}(t_{\text{ini}})$ is determined so that the mass swept up by the forward shock matches the mass of the CSM enclosed with the forward shock, i.e., the following equation

$$\int_{r_{\text{cd}}}^{r_{\text{fs}}} 4\pi r^2 \rho dr = \int_0^{r_{\text{fs}}} 4\pi r^2 \rho_{\text{CSM}} dr, \quad (11)$$

determines $r_{\text{fs}}(t_{\text{ini}})$. Here r_{cd} denotes the radius of the contact discontinuity satisfying

$$\int_{r_{\text{rs}}}^{r_{\text{cd}}} 4\pi r^2 \rho dr = \int_{r_{\text{rs}}}^{\infty} 4\pi r^2 \rho_{\text{ej}} dr. \quad (12)$$

The velocities of the reverse shock and the forward shock, and the radiative flux at the forward shock front, are determined so as to satisfy boundary conditions at the contact discontinuity that the velocity, the pressure, and the radiative flux are continuous. Then we can obtain a position $r_{\text{rs(fs)}}(t + dt)$ at the next time step as $r_{\text{rs(fs)}}(t + dt) = r_{\text{rs(fs)}}(t) + u_{\text{rs(fs)}}(t) dt$.

We stop the calculation when the temperature of a certain shocked region decreases

down to 6000 K, below which most of free electrons recombine.

2.3 Radiative transfer calculations in the unshocked CSM

Radiation emitted from the shocked region diffuses out in the dense unshocked CSM. We solve radiative transfer equations in the unshocked CSM with the luminosities at the forward shock derived in the previous section as boundary conditions. Although radiation may change the structure of matter through which it propagates, we ignore effects of such changes on the radiative transfer. We carry out simplified two-temperature radiative transfer calculations described as below,

$$\frac{\partial E}{\partial t} + \frac{\partial(r^2 F)}{r^2 \partial r} = 4\pi\eta - \kappa\rho cE, \quad (13)$$

$$F = -\frac{c}{(\kappa + \sigma)\rho} \lambda \frac{\partial E}{\partial r}, \quad (14)$$

$$\lambda = \frac{2 + R}{6 + 3R + R^2}, \quad R = \frac{|\partial E / \partial r|}{(\kappa + \sigma)\rho E}, \quad (15)$$

$$\rho \left(\frac{\partial}{\partial t} + v_w \frac{\partial}{\partial r} \right) U + \rho p_{\text{gas}} v_w \frac{\partial \rho^{-1}}{\partial r} = \kappa\rho cE - 4\pi\eta, \quad (16)$$

$$4\pi\eta = \kappa\rho a c T_{\text{gas}}^4, \quad (17)$$

where we use the flux-limited diffusion approximation by Levermore & Pomraning (1981). This formalism satisfies the condition that $|F|$ approaches to cE in the optically thin limit and that equation (14) converges to the diffusion approximation in the optically thick limit. The specific internal energy of gas is denoted by $U = 3kT_{\text{gas}}/2\mu m_{\text{u}}$, the gas pressure p_{gas} , and E is the radiation energy density, which can be expressed with a radiation temperature T_{rad} as $E = aT_{\text{rad}}^4$. Saha's equations shown below give us the mean molecular weight as $\mu^{-1} = X(1 + n_{\text{HIII}}/n_{\text{H}}) + Y/4(1 + n_{\text{HeII}}/n_{\text{He}} + 2n_{\text{HeIII}}/n_{\text{He}})$ with the mass fractions of hydrogen X and helium Y ,

$$\frac{n_{i+1}n_{\text{e}}}{n_i} = \frac{2g_{i+1}}{g_i} \left(\frac{2\pi m_{\text{e}} k T_{\text{gas}}}{h^2} \right)^{3/2} \exp\left(\frac{-\chi_i}{kT_{\text{gas}}} \right), \quad (18)$$

where i denotes the ionization state associated with each element (here we consider gases composed of hydrogen and helium). χ_i is the ionization energy and g_i the statistical weight of ions in an ionization state i . n_{e} and n_i are the number densities of free electrons and ions of the ionization state i . Initial conditions at time $t = t_{\text{ini}}$ for the CSM are set as $T_{\text{gas}}(r, t_{\text{ini}}) = 2000 \text{ K}$, $E(r, t_{\text{ini}}) = 10^{-5} \text{ erg cm}^{-3}$, $F(r_{\text{fs}}, t) = F_{\text{fs}}(t)$, and $F(r > r_{\text{fs}}, t_{\text{ini}}) = cE(r, t_{\text{ini}})$. It should be noted that these initial conditions of the unshocked CSM result in the initial luminosity of the order of $10^{37} \text{ erg s}^{-1}$, which is several orders of magnitude fainter than that from the

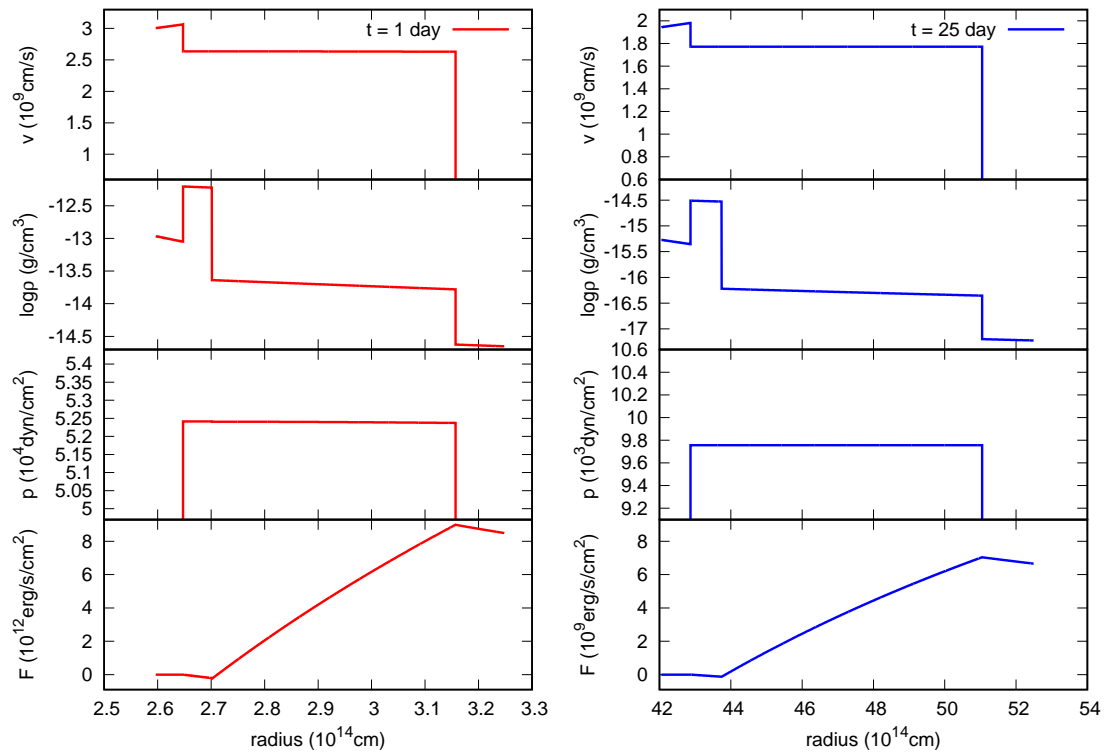


Fig. 1. The structures around the shocked regions at 1 day (the left panels) and 25 day (the right panels) for model SN 2005ip-a. The profiles of velocity, density, pressure, and radiative flux are shown from the top panel to the bottom panel. The reverse and forward shocks at 1 day are located at $r \sim 2.65$ and $\sim 3.15 \times 10^{14}$ cm, respectively. The radiative flux at $r > r_{\text{fs}}$ follows $F \propto r^{-2}$ because the constant luminosity is assumed at $r > r_{\text{fs}}$ in these particular plots.

shocked region.

3 Results and discussion

In this section we show results of our simulations with various parameter sets listed in table 1 and compare some of the resultant LCs with those from other models and well observed SNe II in 2005kj and 2005ip. Throughout our work, we fix ejecta mass of $M_{\text{ej}} = 10M_{\odot}$ (where M_{\odot} is the solar mass) otherwise mentioned.

3.1 Shocked region

Figure 1 shows the inner structure of the shocked region for model SN2005ip-a in table 1 at 1 day and 25 day since explosion. The width of the shocked region increases from $\sim 5 \times 10^{13}$ cm to $\sim 8 \times 10^{14}$ cm during this period while the contact surface moves from 2.7×10^{14} cm to 4.4×10^{15} cm. Thus the small fractional thickness of ~ 0.06 , which remains constant, suggests the validity of the thin shell approximation adopted in Moriya et al.

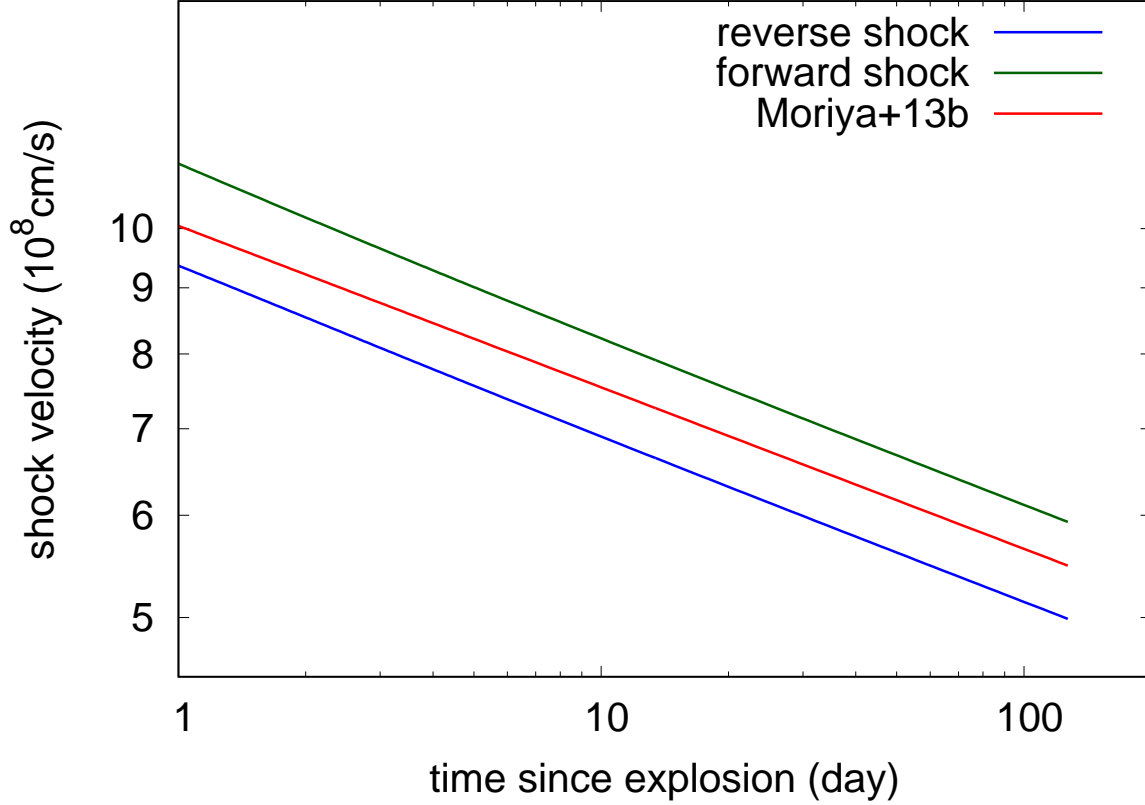


Fig. 2. Velocities of the reverse and forward shocks compared with the velocity of the thin shell derived in Moriya et al. (2013b) as functions of time for the same model in figure 1.

(2013b). This is further supported from a comparison of the velocities of the reverse and forward shocks with the velocity of the thin shell derived by Moriya et al. (2013b) (Figure 2): The velocity of the thin shell runs between the velocities of the forward and reverse shocks, though the thin shell is less decelerated than the shocks. This can be ascribed to radiative loss from the forward shock in our model.

We also calculate the optical depth τ of the shocked region given by,

$$\tau \equiv - \int_{r_{fs}}^{r_{rs}} (\kappa + \sigma) \rho dr, \quad (19)$$

and plot it as a function of time in figure 3. The shocked regions in models E10M10, E1M10, and E1M10n12 keep their optical depths greater than unity until ~ 100 day, while those in models E1M1 and E10M1 becomes optically thin in a few days after explosion. Since the scattering opacity is the dominant source of the total opacity, which is independent of density in high temperature regions, τ is roughly proportional to the density and width of the shocked region. Figure 3 suggests that we can use the diffusion approximation until ~ 100 days after explosion in the dense CSM but for only a few days in the less dense CSM.

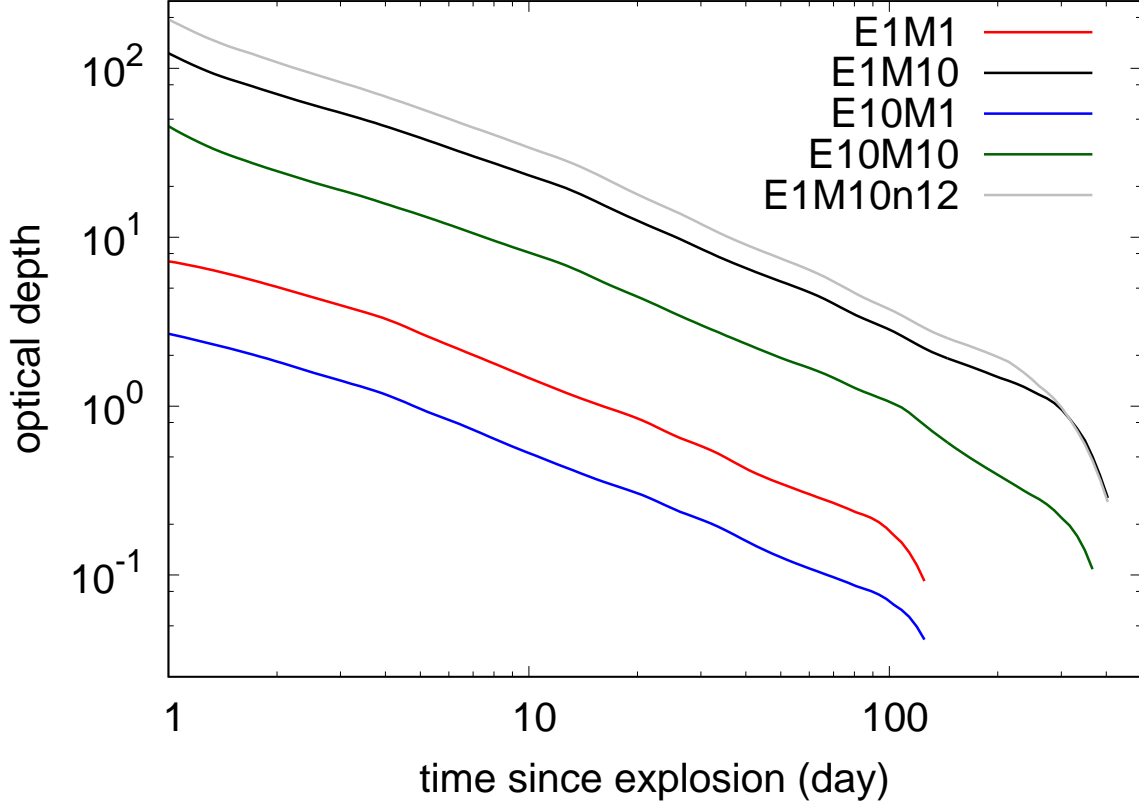


Fig. 3. Optical depth of the shocked region, measured from $r = r_{fs}$ to $r = r_{rs}$ for models indicated by the labels.

3.2 Conversion efficiency

The shock waves dissipate a part of kinetic energy to radiation. The conversion efficiency ϵ from kinetic energy to radiation can be defined as

$$\epsilon = \frac{L}{dE/dt'} \quad (20)$$

where dE/dt is the kinetic energy incident to the shock front per unit time. The efficiency ϵ has been roughly estimated to be ~ 0.1 in the literature (van Marle et al. 2010; Moriya et al. 2013a). The efficiency ϵ at the forward shock front is expressed as

$$\epsilon = \frac{F_{fs}}{\frac{1}{2}\rho_{CSM}u_{fs}^3}. \quad (21)$$

The right hand side of the above equation can be obtained for our models and could be a function of time. The conversion efficiencies of models listed in table 1 are plotted in figure 4 as functions of time. If a SN occurs in dense CSM as in models E10M10, E1M10, and E1M10n12, the conversion efficiency initially takes a high value and decreases for the first several days. Then the conversion efficiency almost keeps a constant value for the

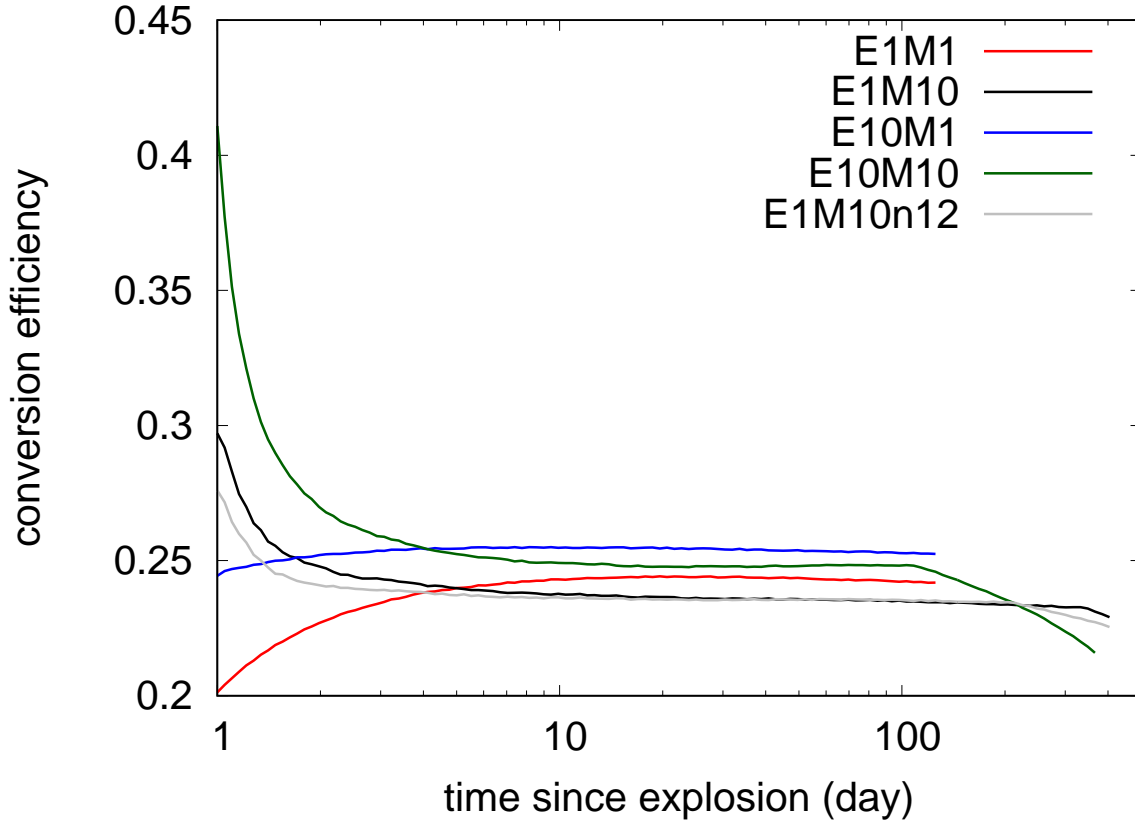


Fig. 4. Conversion efficiencies defined by Equation (21) for several models as functions of time.

subsequent ~ 100 days and abruptly drops at later epochs because the reverse shock enters into the inner ejecta where the density has a shallow profile $\rho_{\text{ej}} \propto r^{-\delta}$ [see equation (7)]. The other models with less dense CSM exhibit different behaviors of the conversion efficiencies. The conversion efficiency gradually increases for the first several days. Then it keeps a constant value till the temperature in the shocked region drops below 6000 K. This is because the reverse shock still stays in the outer ejecta where the density has a steep profile.

Here we will discuss the validity of the LTE assumption by comparing the timescale to emit sufficient photons for thermal radiation estimated by $aT^4/\epsilon_{\text{ff}}$ with other characteristic timescales at the both shock fronts. We consider the free-free emission whose emissivity ϵ_{ff} [$\text{erg s}^{-1} \text{cm}^{-3}$] depends on the density and temperature as

$$\epsilon_{\text{ff}}(\rho, T_{\text{gas}}) \propto \rho^2 T_{\text{gas}}^{1/2}, \quad (22)$$

because photons are mainly generated by free-free emission at the both shock fronts. If the gas in the shocked region attains the LTE state, the emitted radiation energy due to free-free emission exceeds the radiation energy density. Thus $\epsilon_{\text{ff}}(\rho, T_{\text{gas}})t_{\text{min}}/aT^4$ at the shock fronts

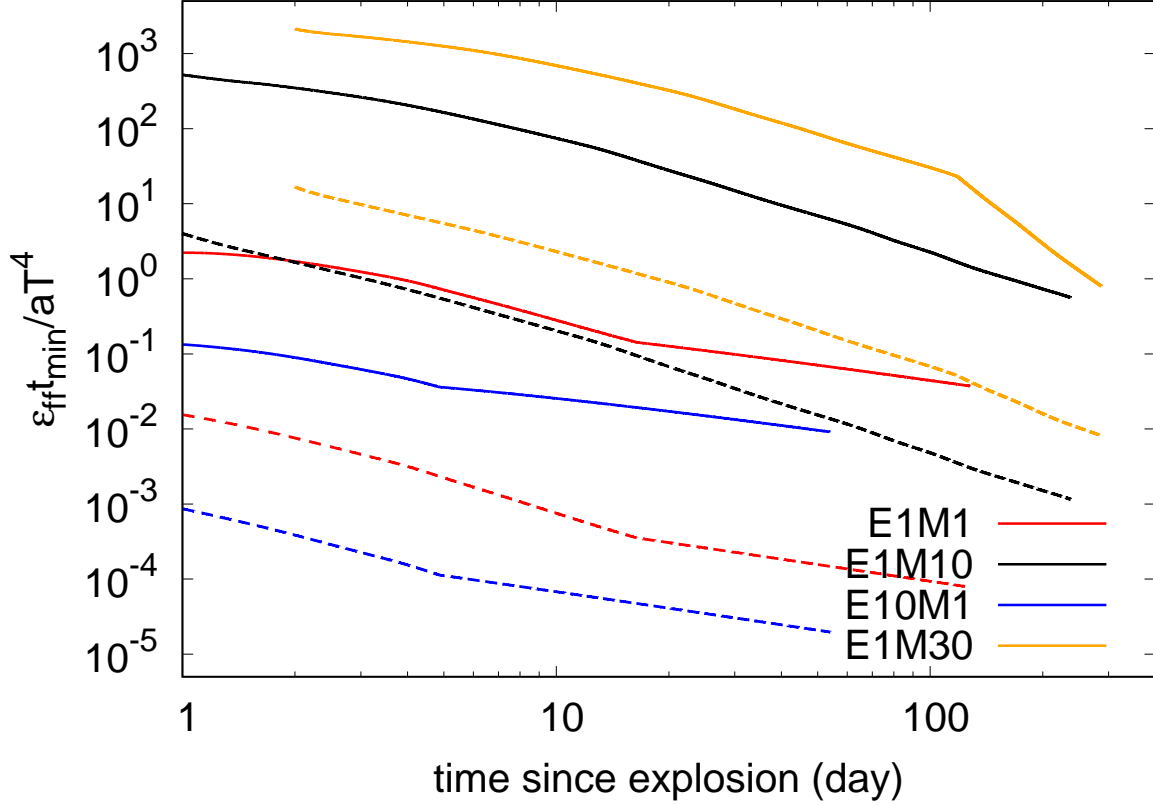


Fig. 5. The values of $\epsilon_{\text{ff}} t_{\text{min}} / aT^4$ at both shock fronts as functions of time for models E1M1, E1M10, E10M1 and E1M30. The solid lines show $\epsilon_{\text{ff}} t_{\text{min}} / aT^4$ at the reverse shock, while the dashed lines at the forward shock. Model E1M30 is calculated from day 2 while others from day 1.

can measure the validity of the LTE assumption, where t_{min} denotes the shortest characteristic timescale. Since the shocked region changes due to the expansion and/or the diffusion of radiation, t_{min} can be estimated from

$$t_{\text{min}} \equiv \min\{t, t_{\text{diff}}\}, \quad (23)$$

$$t_{\text{diff}} \sim \max\{\tau, 1\} \frac{\Delta r}{c}, \quad (24)$$

where $\Delta r \equiv r_{\text{fs}} - r_{\text{rs}}$ is the width of the shocked region. When the total pressure is dominated by the gas pressure, we obtain the gas temperature T_{gas} as below,

$$T_{\text{gas, rs}} \equiv \frac{3}{16} \frac{\mu m_{\text{u}}}{k} (r_{\text{rs}}/t - u_{\text{rs}})^2, \quad (25)$$

$$T_{\text{gas, fs}} \equiv \frac{3}{16} \frac{\mu m_{\text{u}}}{k} (v_{\text{w}} - u_{\text{fs}})^2, \quad (26)$$

which are derived from the equation of state for monoatomic ideal gas. Figure 5 shows $\epsilon_{\text{ff}}(\rho, T_{\text{gas}}) t_{\text{min}} / aT^4$ as functions of time for several models. From this figure, the values of $\epsilon_{\text{ff}} t_{\text{min}} / aT^4$ at the reverse shock in models E1M10 and E1M30 exceed unity throughout

their evolution while $\epsilon_{\text{ff}} t_{\text{min}} / aT^4 < 1$ in model E1M1 and E10M1. Thus the LTE assumption holds at the reverse shock front in models E1M10 and E1M30. On the other hand, the time dependence of $\epsilon_{\text{ff}} t_{\text{min}} / aT^4$ at the forward shock front shows different behaviors. In models E1M10 and E1M30, $\epsilon_{\text{ff}} t_{\text{min}} / aT^4 > 1$ until a few days after the explosion, dropping below unity afterwards. In model E10M1, we cannot assume the LTE state at both reverse and forward shock fronts throughout their evolution. If we impose the condition $\epsilon_{\text{ff}} t_{\text{min}} / aT^4 > 1$ holds at the forward shock for the first $100 \times t_{100}$ days, a dimensional analysis implies that the criterion

$$\left(\frac{M_{\text{ej}}}{M_{\odot}}\right)^{3/4} \left(\frac{E_{\text{ej}}}{10^{51} \text{ erg}}\right)^{-3/4} \left(\frac{\dot{M}}{M_{\odot} \text{ yr}^{-1}}\right) \gtrsim 0.6 t_{100}, \quad (27)$$

should be satisfied. Thus our model can be applied to SNe IIn interacting with very dense CSM with a mass-loss rate $\gtrsim 0.1 M_{\odot} \text{ yr}^{-1}$ for a SN with $M_{\text{ej}} \sim 10 M_{\odot}$ and $E_{\text{ej}} \sim 10^{51} \text{ erg}$, for example.

3.3 Light curves

Figure 6 shows LCs calculated from the luminosity at the outer edge of CSM located at $r_{\text{out}} = 10^{16} \text{ cm}$. SNe IIn are brighten as photons emitted from the shocked region diffuse out from the CSM. Thus if we compare models E1M1 and E1M10, model E1M10 with denser CSM has a wider peak in its LC and a higher peak luminosity as shown in this figure. More energetic ejecta result in an earlier time of the peak luminosity and a higher peak as seen from a comparison of models E1M10 and E10M10. More rapid expansion of the shocked region shortens the diffusion time of photons in the CSM. This is the reason why a factor of 10 energetic model has more than a factor of 10 higher peak luminosity. Afterwards, the luminosity declines following the same power law as that of Moriya et al. (2013b) until the reverse shock enters the inner ejecta.

3.3.1 Comparison with Tsuna et al. (2019)

To check the validity of assumptions made in our models, we compare our models E1M10 and E1M30 with other models in Tsuna et al. (2019), which used the same setup for the initial conditions. In figure 7, we compare our LCs with those derived by Tsuna et al. (2019). Models E1M10 and E1M30 have dimmer peak luminosities compared with Tsuna et al. (2019), while the initial rise time is similar. In our models, a part of radiation energy heats up the unshocked CSM and thus the luminosity is reduced. Tsuna et al. (2019) did not take into account this effect. We will estimate how much radiation energy ΔE is used to heat

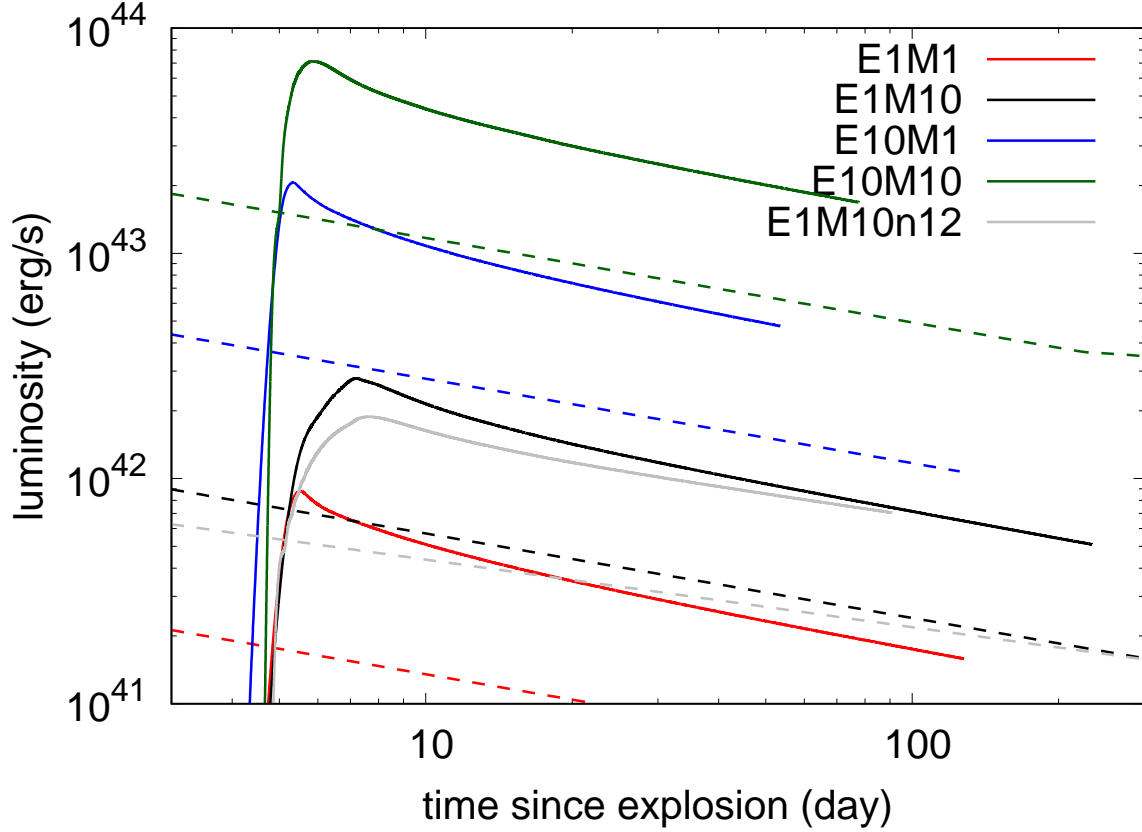


Fig. 6. Calculated LCs measured at the edge of the unshocked CSM (solid line). Dashed lines are the LCs by Moriya et al. (2013b). Lines with the same color correspond to the same parameter set.

up the unshocked CSM by the following formula.

$$\Delta E \sim \int (L_{\text{fs}} - L(r = r_{\text{out}})) dt, \quad (28)$$

where L_{fs} denotes the luminosity emergent from the forward shock and calculated as $L_{\text{fs}} = 4\pi r_{\text{fs}}^2 F_{\text{fs}}$ and $L(r)$ denotes the luminosity distribution. We obtain values of $\Delta E \sim 5.4 \times 10^{47}, 1.6 \times 10^{48}$ erg for models E1M10 and E1M30, respectively. If ΔE were emitted as radiation over a certain time Δt , peak luminosity L_p would increase by $\Delta E / \Delta t$. If Δt is characterized by the initial rise time, $\Delta E / \Delta t \sim 2 \times 10^{42}, 3 \times 10^{42}$ ergs^{-1} for models E1M10 and E1M30, respectively. These values could explain the difference between the models compared in figure 7. Thus the heating of the CSM and resultant reduction of the emergent flux should be taken into account when calculating the luminosity around the peak.

The assumption of LTE of our models overestimates the radiative flux after the region becomes optically thin as seen from the tails brighter than those of Tsuna et al. (2019). From figure 5, $\epsilon_{\text{ff}} t_{\text{min}} / aT^4$ at the reverse shock front exceeds unity in both models. By contrast, at the forward shock $\epsilon_{\text{ff}} t_{\text{min}} / aT^4 \lesssim 1$ in both models at later epochs as discussed in section

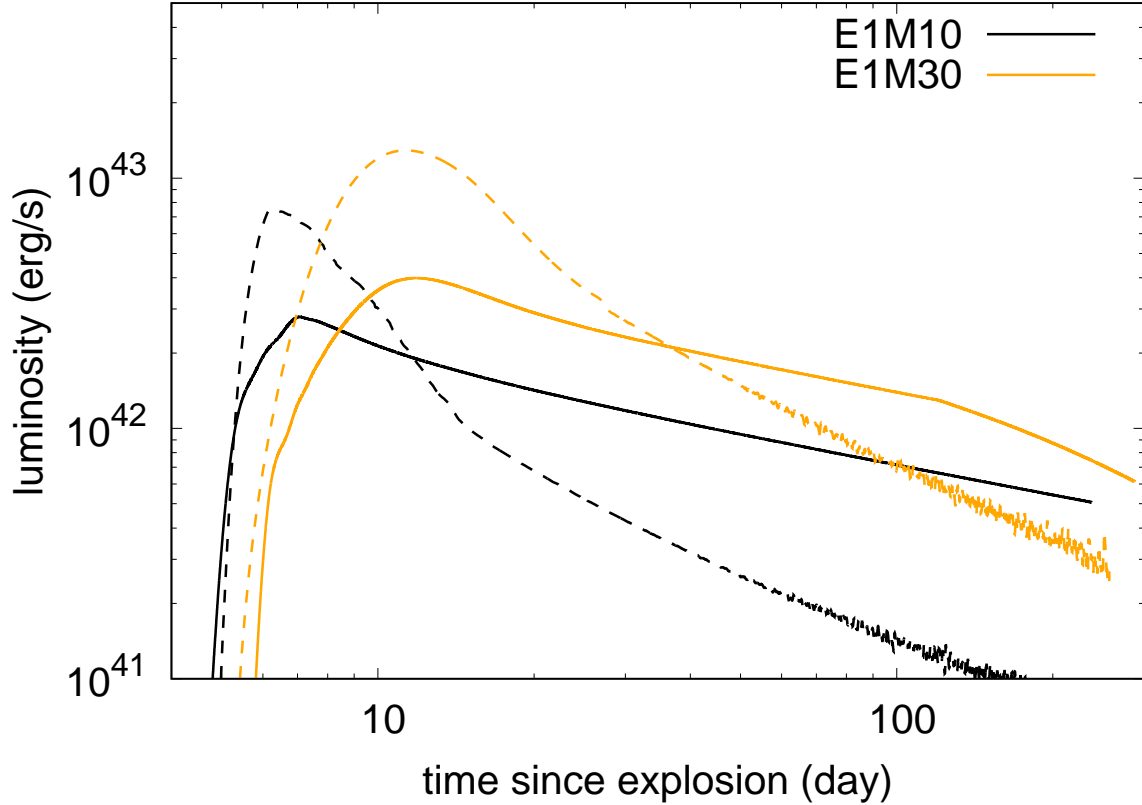


Fig. 7. Comparison of our models (solid line) with models by Tsuna et al. (2019) (dashed line). The lines with the same color correspond to models with the same parameter set.

3.2, which also leads to the overestimation of the luminosity. The luminosity of our model follows power-law evolution until the reverse shock enters the inner ejecta, while the luminosity of models by Tsuna et al. (2019) shows steeper drop in the optically thin phase due to the more properly treated emission process.

3.4 Comparison with observations

Here we compare our results with two well observed SNe 2005kj and 2005ip. We show what kind of information we can obtain and discuss the limitation of our model.

3.4.1 SN 2005kj

We have picked up this SN because the mass-loss rate of the progenitor was estimated to be $\sim 0.9 M_{\odot} \text{ yr}^{-1}$ (Moriya et al. 2014). This high mass loss rate indicates that this SN may satisfy the criterion (27).

To reproduce the bolometric LC of SN 2005kj constructed from optical and near-

infrared observations (Taddia et al. 2013) as shown in figure 8, we need to assume the explosion date 20 days before the discovery. The LC of this SN has a break at $t \sim 100$ d (We will refer this epoch to t_t). We found that most of the emission after this epoch comes from the shocks having already entered the inner core to reproduce the rapidly dropping flux. Thus the value of δ affects the shape of the LC and is found to be 1.5 to reproduce the observed LC. The best fit model (SN 2005kj-a) requires the other exponents to be $(n, s) = (7, 1.2)$ and the energy of $E_{ej} = 6.3 \times 10^{50}$ erg. The CSM density distribution of the best fit model is given by

$$\rho_{\text{CSM}}(r) \simeq 9.7 \times 10^{-14} \left(\frac{r}{10^{15} \text{ cm}} \right)^{-1.2} \text{ g cm}^{-3}. \quad (29)$$

Since s is not equal to 2, the required mass loss is not stationary. We define the average value as

$$\begin{aligned} \langle \dot{M} \rangle &\equiv \frac{v_w}{r_{\text{out}}} \int_{R_p}^{r_{\text{out}}} 4\pi r^2 \rho_{\text{CSM}} dr \\ &\simeq \frac{4\pi D v_w}{3-s} r_{\text{out}}^{2-s}, \end{aligned} \quad (30)$$

where R_p ($\ll r_{\text{out}}$) is the progenitor radius and D denotes the proportional constant of the density of the CSM. From equations (29) and (30), we obtain the mean mass-loss rate of $\langle \dot{M} \rangle \simeq 0.39 (r_{\text{out}} / (5 \times 10^{15} \text{ cm}))^{0.8} M_{\odot} \text{ yr}^{-1}$. This value is of the same order of magnitude as that derived by Moriya et al. (2014). Such a high CSM density satisfies the criterion (27), thus the assumption of LTE state can be justified throughout the evolution of SN 2005kj shown in this figure.

Figure 8 also shows the other three models SN 2005kj-b, c, d compared with the plot of the bolometric LC of SN 2005kj. If we change E_{ej} from 6×10^{50} erg to 10^{51} erg (model SN 2005kj-b) without changing the other parameters from model SN 2005kj-a, the break point t_t appears ~ 20 days earlier than in model SN 2005kj-a and the luminosity drops faster at later times. On the other hand, δ affects t_t and the luminosity at $t \geq t_t$ while it does not change the luminosity at early phase so much. Model SN 2005kj-c with a larger δ exhibits a shorter t_t and flatter luminosity at later times, as shown in figure 8. Moreover, we change s from 1.2 to 2 in model SN 2005kj-d while keeping the averaged mass-loss rate $0.39 M_{\odot} \text{ yr}^{-1}$ and the other parameters the same, which yields the CSM density of

$$\rho_{\text{CSM}}(r) \simeq 2.0 \times 10^{-13} \left(\frac{r}{10^{15} \text{ cm}} \right)^{-2} \text{ g cm}^{-3}. \quad (31)$$

As compared with model SN 2005kj-a, the luminosity of SN 2005kj-d is significantly fainter at all times as shown in figure 8. This is considered to be caused by absorption of radiation

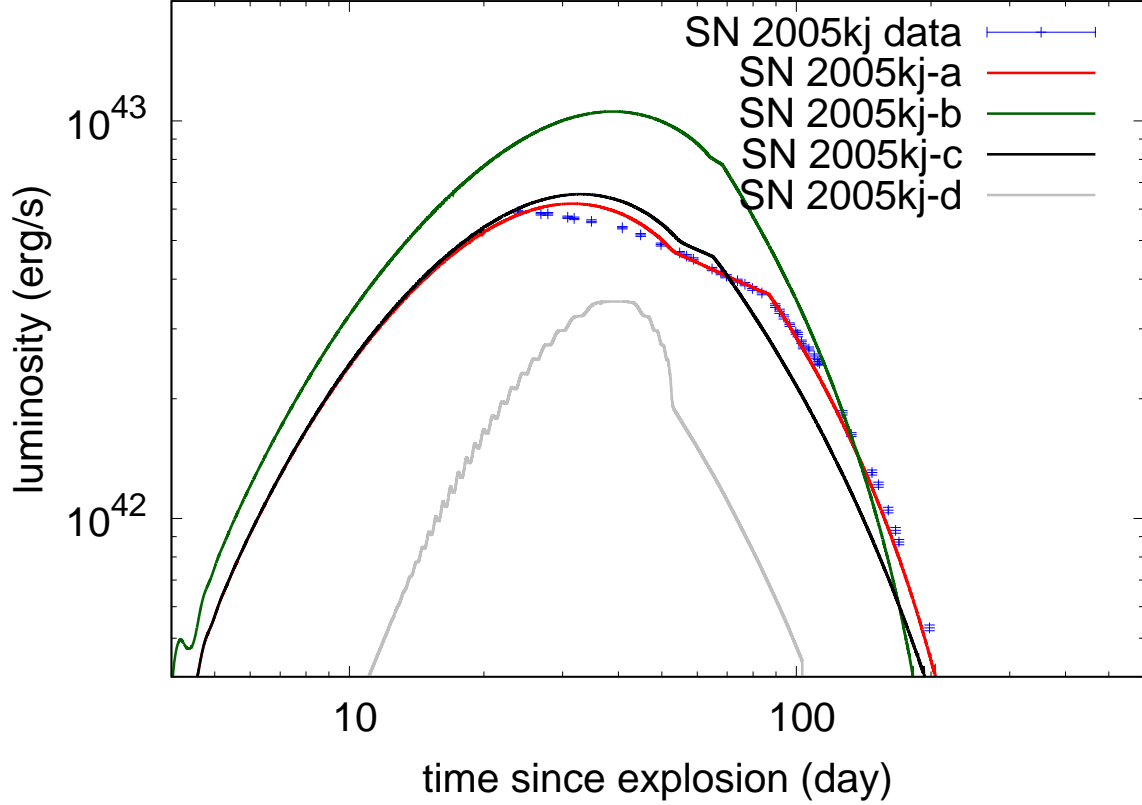


Fig. 8. Comparison of the observational data of SN 2005kj with our numerical models.

in the CSM, which can be seen from a difference in the column densities between these two models. In order to confirm this, we compare the column density $N(s)$ of model SN 2005kj-d with that of model SN 2005kj-a, calculated as

$$\begin{aligned}
 N(s) &\equiv \int_{r_{\text{fs}}(t_{\text{ini}})}^{r_{\text{out}}} \rho_{\text{CSM}} dr \\
 &= \frac{D}{s-1} \left[r_{\text{fs}}(t_{\text{ini}})^{1-s} - r_{\text{out}}^{1-s} \right].
 \end{aligned} \tag{32}$$

This equation yields $N(2) \simeq 2 \times 10^3 \text{ g cm}^{-2}$ while $N(1.2) \simeq 3 \times 10^2 \text{ g cm}^{-2}$, which is smaller than $N(2)$ by a factor of 10. This larger $N(2)$ indicates that more radiation from the shocked region is absorbed in the CSM rather than reaching the observer. For instance, the inner region of CSM, i.e. at $r = 10^{14} \text{ cm}$ in model SN 2005kj-d, is an order of magnitude denser than in SN 2005kj-a while these are comparable at $r = 10^{15} \text{ cm}$. This means that much more radiation could be absorbed by this denser region and thus the emergent luminosity becomes fainter.

3.4.2 SN 2005ip

SN 2005ip is another well-studied SN II_n (e.g., Smith et al. 2009; Stritzinger et al. 2012). The wind velocity and mass-loss rate are estimated to be $\sim 100 \text{ km s}^{-1}$ and $2.2 \times 10^{-4} M_{\odot} \text{ yr}^{-1}$ by Smith et al. (2009). Moriya et al. (2013b) fitted a power law function:

$$L \propto t^{\alpha}, \quad (33)$$

with an exponent α to the observed LC and obtained $\alpha = -0.536$. This exponent is a function of n and s expressed as

$$\alpha = \frac{6s - 15 + 2n - ns}{n - s}. \quad (34)$$

Then they derived two parameter sets of $(E_{\text{ej},51}, \dot{M}_{-3}, n, s) = (13, 1.2, 10, 2.3)$ and $(15, 1.4, 12, 2.4)$ with $v_w = 100 \text{ km s}^{-1}$ and $r_{\text{out}} = 10^{16} \text{ cm}$ for two different structures of the progenitor ($n = 10$ and 12). The temporal evolution of shock velocity and luminosity of our model at later epochs is almost the same as that of Moriya et al. (2013b).

Thus, at first we fit the analytical model by Moriya et al. (2013b) to the observational data of SN 2005ip at later epochs and obtain $\alpha \simeq -0.447$. This is greater than the original value obtained in Moriya et al. (2013b) because we ignored the LC in the early phase ($t < 30$ day) that is affected by the photon diffusion in the CSM. From equation (34), we obtain $s \simeq 2.13$ when $n = 10$. Assuming the steady mass-loss ($s = 2$), n becomes about $n \simeq 8.7$. Furthermore, in order to restrict the parameters we fit the calculated shock velocity. This procedure is the same as that of Moriya et al. (2013b). From evolution of the width of the $\text{H}\alpha$ profile, it is found that the shock velocity is $\sim 1.8 \times 10^4 \text{ km s}^{-1}$ at $\sim 10 - 100$ day (Stritzinger et al. 2012). Our best fit model suggests $E_{\text{ej}} \simeq 8.1 \times 10^{51} \text{ erg}$, which is smaller than $E_{\text{ej}} \simeq 1.3 \times 10^{52} \text{ erg}$ (Moriya et al. 2013b) and

$$\rho_{\text{CSM}}(r) \simeq 1.5 \times 10^{-18} \left(\frac{r}{10^{16} \text{ cm}} \right)^{-2.13} \text{ g cm}^{-3}. \quad (35)$$

Our model suggests a conversion efficiency higher than 0.1 and thus can reduce the kinetic energy of SN ejecta. LCs with these parameters at $r = r_{\text{out}}, r_{\text{fs}}$ are plotted in figure 9 as well as the observational data of SN 2005ip. From equations (30) and (35) we obtain $\langle \dot{M} \rangle \simeq 3.2 \times 10^{-4} (r_{\text{out}} / (10^{16} \text{ cm}))^{-0.13} M_{\odot} \text{ yr}^{-1}$. This low average value casts doubt on the validity of our assumption of the LTE according to the criterion given in formula (27). This means that we underestimated the mass-loss rate. In fact, Tsuna et al. (2019) estimated the mass-loss rate as $\langle \dot{M} \rangle \simeq 1 \times 10^{-2} M_{\odot} \text{ yr}^{-1}$ ($E_{\text{ej}} = 1.5 \times 10^{52} \text{ erg}$) from the LC fitting by their model, which partially takes into account the finite time to achieve the LTE. Thus we need to explicitly incorporate emission and absorption processes in the formulation for the shocked region as

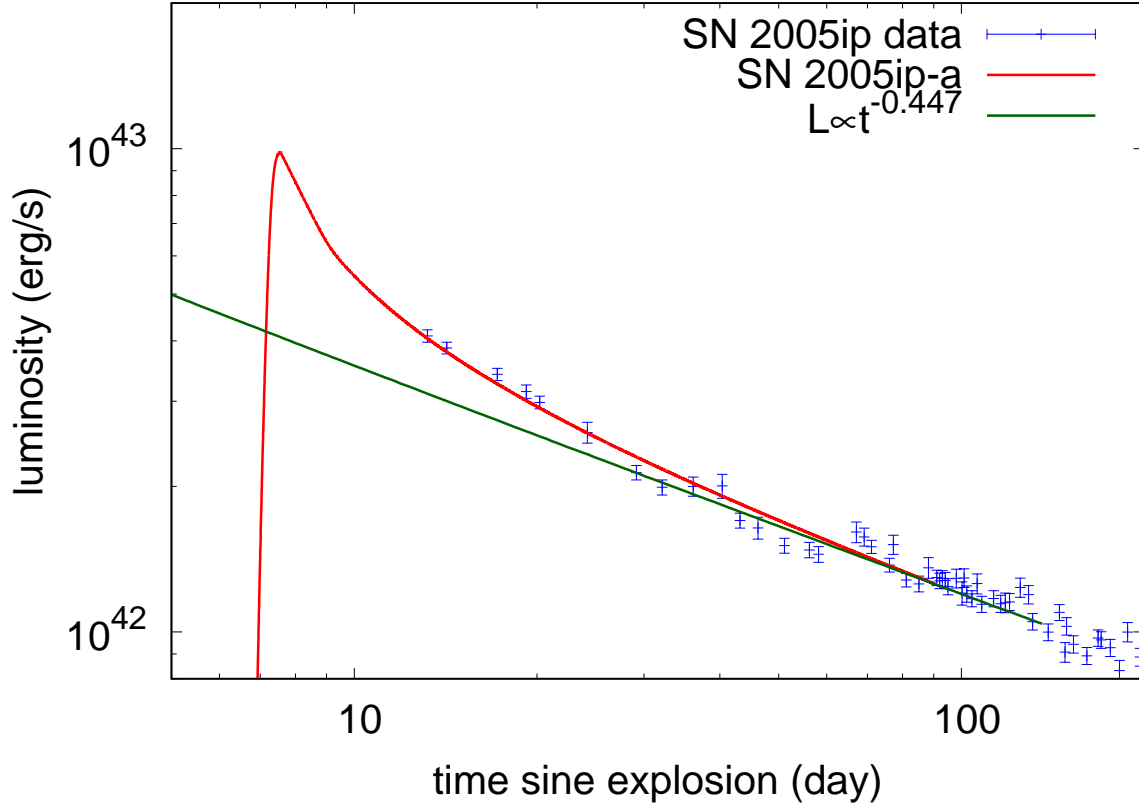


Fig. 9. Comparison of the observational data of SN 2005ip with our numerical model SN 2005ip-a.

was done for the CSM to obtain physical parameters by comparison with this particular SN LC data with our model.

4 Conclusion and future perspective

We successfully constructed a model that guarantees to spatially resolve structures in the shocked region between SN ejecta and CSM, assuming a steady state in the rest frame of each of the shocks and calculate radiative transfer equations and energy equation to derive the luminosity at the outer edge of the CSM. We assumed the LTE in the shocked region to avoid numerical instabilities associated with integration with respect to the radial coordinate, while we explicitly included terms describing radiative emission and absorption in the CSM. By doing so, we can predict the peak luminosity of a SN IIn for thick CSM. Thus the structure of CSM can be inferred from observed initial rise times of the LC of a SN IIn. As discussed in section 3.3.1, the unshocked CSM plays a crucial role in reducing radiative flux emergent from a forward shock front.

In the near future, we can test our model by a large number of observational data

in the early phase of SNe IIn, or the peak luminosity, which will be detected by exceedingly wide-field and high-cadence optical camera Tomo-e Gozen and/or Zwicky Transient Facility (e.g., Sako et al. 2016; Smith et al. 2014). From these facilities we will be able to study the relationship between the initial rise times and the peak luminosities of SNe IIn.

We found that the assumption of LTE near the forward shock is broken in models with mass-loss rates often inferred from SNe IIn. In the next step we need to take into account radiative absorption and emission processes in the shocked region. This could be done if we succeed in suppressing numerical instabilities associated with the integration of the energy equation with respect to the radius in the shocked region. We will try an implicit method to integrate the energy equation to see if we can suppress the instabilities.

Though we assume spherical symmetry throughout the paper, many observations about the geometry of CSM have revealed that those of some progenitors of SNe IIn have aspherical structures (e.g., Leonard et al. 2000; Hoffman et al. 2008; Katsuda et al. 2016). Suzuki et al. (2019) calculated 2D radiation hydrodynamic simulations for a spherical ejecta colliding with the circumstellar disk. Our method may be applicable to this large scale asphericity by using aspherical CSM structures and/or aspherical ejecta structures. To do so, we need to include components of radiative flux and velocity in the other directions. This is rather straightforward, though the formulation becomes much more complicated. In addition, we need to treat the asphericity caused by turbulent motion of gas, which will develop to smaller scales. This requires a high spatial resolution and may weaken the feasibility of our method.

Acknowledgments

The authors thank Takashi J. Moriya for giving the observational bolometric light curve data of SN 2005kj and SN 2005ip to us. The authors also appreciate that Daichi Tsuna gives us the results of his numerical simulations. YT is supported by RIKEN Junior Research Associate Program. YT is profoundly grateful to Daichi Tsuna for the discussion. This work is partially supported by JSPS KAKENHI Grant Numbers 16H06341, 16K05287, 15H02082, MEXT, Japan.

References

- Arnett, W. D. 1980, *ApJ*, 237, 541
- Castor, J. I., Abbott, D. C., & Klein, R. I. 1975, *ApJ*, 195, 157
- Chatzopoulos, E., Wheeler, J. C., & Vinko, J. 2012, *ApJ*, 746, 121
- Chevalier, R. A. 1982, *ApJ*, 258, 790
- Chevalier, R. A., & Irwin, C. M. 2011, *ApJL*, 729, L6

Dessart, L., Audit, E., & Hillier, D. J. 2015, *MNRAS*, 449, 4304

Filippenko, A. V. 1997, *ARA&A*, 35, 309

Förster, F., et al. 2018, *Nature Astronomy*, 2

Ginzburg, S., & Balberg, S. 2012, *ApJ*, 757, 178

Hoffman, J. L., Leonard, D. C., Chornock, R., Filippenko, A. V., Barth, A. J., & Matheson, T. 2008, *ApJ*, 688, 1186

Iglesias, C. A., & Rogers, F. J. 1996, *ApJ*, 464, 943

Katsuda, S., et al. 2016, *ApJ*, 832, 194

Leonard, D. C., Filippenko, A. V., Barth, A. J., & Matheson, T. 2000, *ApJ*, 536, 239

Levermore, C. D., & Pomraning, G. C. 1981, *ApJ*, 248, 321

Marigo, P., & Aringer, B. 2009, *A&A*, 508, 1539

Matzner, C. D., & McKee, C. F. 1999, *ApJ*, 510, 379

Moriya, T. J., Blinnikov, S. I., Tominaga, N., Yoshida, N., Tanaka, M., Maeda, K., & Nomoto, K. 2013a, *MNRAS*, 428, 1020

Moriya, T. J., Maeda, K., Taddia, F., Sollerman, J., Blinnikov, S. I., & Sorokina, E. I. 2013b, *MNRAS*, 435, 1520

—. 2014, *MNRAS*, 439, 2917

Sako, S., et al. 2016, in *Society of Photo-Optical Instrumentation Engineers (SPIE) Conference Series*, Vol. 9908, Proc. SPIE, 99083P

Schlegel, E. M. 1990, *MNRAS*, 244, 269

Smith, N. 2014, *ARA&A*, 52, 487

Smith, N., & Owocki, S. P. 2006, *ApJL*, 645, L45

Smith, N., et al. 2009, *ApJ*, 695, 1334

Smith, R. M., et al. 2014, in *Society of Photo-Optical Instrumentation Engineers (SPIE) Conference Series*, Vol. 9147, Proc. SPIE, 914779

Stritzinger, M., et al. 2012, *ApJ*, 756, 173

Suzuki, A., Moriya, T. J., & Takiwaki, T. 2019, arXiv e-prints, arXiv:1911.09261

Taddia, F., et al. 2013, *A&A*, 555, A10

Tsuna, D., Kashiyama, K., & Shigeyama, T. 2019, *ApJ*, 884, 87

van Marle, A. J., Smith, N., Owocki, S. P., & van Veelen, B. 2010, *MNRAS*, 407, 2305

Table 1. Models and input parameters.

Model	n	s	δ	$E_{\text{ej},51}^*$	\dot{M}_{-3}^\dagger
E1M1	10	2	1	1	1
E10M1	10	2	1	10	1
E1M10	10	2	1	1	10
E1M30	10	2	1	1	30
E10M10	10	2	1	10	10
E1M10n12	12	2	1	1	10
SN 2005kj-a [‡]	7	1.2	1.5	0.63	390
SN 2005kj-b	7	1.2	1.5	1	390
SN 2005kj-c	7	1.2	2	0.63	390
SN 2005kj-d	7	2	1.5	0.63	390
SN 2005ip-a [‡]	10	2.13	1	8.1	0.32

* Kinetic energy in units of 10^{51} erg.

† Mass-loss rate in units of $10^{-3}M_{\odot}\text{yr}^{-1}$. If $s \neq 2$, the average values defined in equation (30) are shown.

‡ Models for SNe 2005kj and 2005ip.